Mosquito breeding site water temperature observations and simulations towards improved vector-borne disease models for Africa

Ernest O. Asare,[1,2] Adrian M. Tompkins,[2] Leonard K. Amekudzi,[1] Volker Ermert,[3] Robert Redl[4]

[1]Department of Physics, Kwame Nkrumah University of Science and Technology, Kumasi, Ghana; [2]Abdus Salam International Centre for Theoretical Physics, Trieste, Italy; [3]Institute of Geophysics and Meteorology, University of Cologne; [4]Meteorological Institute, Ludwig-Maximilians-University, Munich, Germany

Abstract

An energy budget model is developed to predict the water temperature of typical mosquito larval developmental habitats. It assumes a homogeneous mixed water column driven by empirically derived fluxes. The model shows good agreement at both hourly and daily time scales with 10-min temporal resolution observed water temperatures, monitored between June and November 2013 within a peri-urban area of Kumasi, Ghana. There was a close match between larvae development times calculated using either the model-derived or observed water temperatures. The water temperature scheme represents a significant improvement over assuming the water temperature to be equal to air temperature. The energy budget model requires observed minimum and maximum temperatures, information that is generally available from weather stations. Our results show that hourly variations in water temperature are important for the simulation of aquatic-stage development times. By contrast, we found that larval development is insensitive to sub-hourly variations. Modelling suggests that in addition to water temperature, an accurate estimation of degree-day development time is very important to correctly predict the larvae development times. The results highlight the potential of the model to predict water temperature of temporary bodies of surface water. Our study represents an important contribution towards the improvement of weather-driven dynamical disease models, including those designed for malaria early forecasting systems.

Introduction

Temperature is one important abiotic factor that influences the life cycle of the malaria parasite and its Anopheles mosquito vectors (Detinova, 1962; Garrett-Jones and Grab, 1964; Kirby and Lindsay, 2004). Aquatic stage developmental rate is highly temperature dependent. At low water temperatures, adults fail to emerge while high water temperatures are associated with high larvae mortality rates.

Many laboratory experiments have been conducted to understand how water temperature influences the aquatic life cycle of mosquitoes. Bayoh and Lindsay (2003) showed that *Anopheles gambiae sensu stricto* emerged as adults only when water temperatures ranged between 18 and 34°C. The optimum temperature in which development of *Anopheles gambiae* larvae is favoured was found to be 27°C by Lyimo *et al.* (1992) in the laboratory. Bayoh and Lindsay (2004) showed that no adult *An. gambiae* mosquito emerged from larvae reared below 18 and above 32°C.

Water temperature also controls larval longevity and survival. For instance, Bayoh and Lindsay (2004), observed the larval survival of *An. gambiae*. It ranged between 10 and 38 days at a constant temperature of 18°C whereas at 32°C longevity varied between 5 and 13 days. Similarly, Kirby and Lindsay (2009) observed rapid development rates but decreases in survival rates with an increase in water temperature for both *An. gambiae* and *Anopheles arabiensis*. At the upper temperature threshold where development time is short, it is associated with a high larval mortality rate (Bayoh and Lindsay, 2004; Kirby and Lindsay, 2009).

Including a realistic representation of the vector immature stage and its water temperature sensitivity could potentially improve the

accuracy of disease transmission models. Lunde *et al.* (2013a) argued that including water temperature effects in transmission models significantly reduces the temperature range at which peak transmission takes place. The latter is often estimated for adult vector mortality rates combined with the temperature-dependency of the sporogonic cycle (Craig *et al.*, 1999).

Many spatial, dynamical mathematical-biological malaria models lack a precise simulation of water temperatures. For instance, in the Liverpool malaria model (Hoshen and Morse, 2004; Ermert *et al.*, 2011a, 2011b) the aquatic stage duration is constant in the model. The dynamical model (VECTRI; Tompkins and Ermert, 2013) simply equates mean air temperature to water temperature to drive the aquatic stage component of the model.

Paaijmans *et al.* (2008a) demonstrated that mean water temperature was higher than that of ambient air temperature. Paaijmans *et al.* (2010) and Paaijmans and Thomas (2013) found for Kenya that mean water temperatures of potential breeding habitats were 4-6°C higher than corresponding mean air temperatures. The implication of this result is that using air temperature to predict the aquatic life span of mosquitoes is inaccurate and that the application of a water temperature parameterisation scheme would improve dynamical vector-borne disease models. Some attempts have been made to develop more complex representations of water temperature. Lunde *et al.* (2013b) equated the mean breeding water temperature to topsoil temperature. Depinay *et al.* (2004) introduced a simple water temperature scheme, using relative humidity as well as minimum and maximum air temperatures. Neither the Lunde *et al.* (2013b) nor Depinay *et al.* (2004) schemes were evaluated using *in situ* data.

Energy balance models have also been used to predict water temperature. Losordo and Piedrahita (1991) developed an energy balance model to predict temperature of stratified aquaculture ponds. Paaijmans *et al.* (2008a) developed a model that predicts the diurnal water temperature based on radiation and energy fluxes of air-water and soil-water. This model was further simplified by Paaijmans *et al.* (2008b) to use only easily obtained weather data as input, but even this modified scheme still required cloud cover observations to compute incoming shortwave radiation, a parameter not readily available from most meteorological stations.

The aim here was to develop an energy balance parameterisation scheme using approximations such that the model can be driven using only common observed meteorological variables from weather stations. In addition, rather than evaluating the model with measurements at artificial sites, the goal was to predict the actual mosquito habitat water temperatures that were monitored using high temporal resolution field observations in Kumasi, Ghana. After data collection, we first assessed the performance of the model to predict water temperature. Secondly, we predicted larvae development times using a dynamical malaria model. Thirdly, we estimated the impact of water temperature errors on larvae development times and densities of a malaria transmission model.

Materials and Methods

Study area and data

The study was conducted at the Kwame Nkrumah University of Science and Technology (KNUST) campus, within the Kumasi Metropolis of Ghana (0.85342° W, 5.95248° N). Between 01 June [day of the year (DOY) 152] and 26 November 2013 (DOY 330) a 10-min water temperatures of three mosquito developmental habitats were

observed using a CR1000 data logger (Campbell Scientific Ltd., Shepshed, UK) with PT-100 temperature sensors. The probes of the temperature sensor were placed 1 cm below the surface of the water. These three observed ponds were made up of trenches between raised beds for lettuce cultivation (Figure 1). In addition, these observed ponds were completely exposed to sunlight. During the observational period, there were 63 (34%), 66 (36%) and 85 (46%) days where ponds dried out completely for site 1, site 2 and site 3, respectively. It is recalled that *An. gambiae,* the key vector in Kumasi (De Souza *et al.*, 2010) and *An. arabiensis* prefer sunlit pools (Minakawa *et al.*, 1999; Gimnig *et al.*, 2001; Koenraadt *et al.*, 2004) and thus modeling such habitats is considered key.

During the same period, various climatic input variables (temperature, wind speed, relative humidity and pressure) were obtained from the KNUST Energy Centre Automatic Weather Station (AWS), located about 300 metres away from the pond sites (0.85230° W, 5.9524° N). These variables were also recorded by an AWS logger at 10-min temporal resolution. The 10-min water temperature and climatic input datasets were averaged into hourly and daily time scales for this study. In addition, the water depth was set to the average of four measurements taken at fixed locations within each pond.

Energy balance model for water temperature

Solar radiation, longwave radiation, latent, sensible and ground heat fluxes are the main components that control the amount of heat that is stored in or released from a water column (Figure 2). The water column in this model is assumed to be well mixed at all times, such that temperature is independent of depth and diffusive and convective transports are ignored. The rate of change of heat storage per unit area (*Q*) is given by eq. 1.

$$\frac{dQ}{dt} = R_{net} - LH - SH - G_o \qquad \text{(eq. 1)}$$

where: R_{net} is the net radiative flux (that is sum of net solar and long-wave radiation); *LH* represents the latent heat flux; *SH* the sensible heat flux; and G_o is the soil heat flux.

For simplicity, it is assumed that the pond water is sufficiently turbid

Figure 1. Picture of study site showing the temperature logger.

such that all solar radiative fluxes are absorbed in the water column and no transmission occurs. Thus the only transfer of energy to the sediment layer is G_o. In addition, the sensible heat flux associated with the temperature of raindrops being lower than the water temperature is also neglected. Gosnell *et al.* (1995) estimated this to be of the order of 2.5 W m^{-2} over tropical oceans and thus small compared with other terms. Nevertheless, in periods of intense rainfall, this flux can exceed 200 W m^{-2} and thus its neglect may lead to overestimation of water temperatures at these times. Fluxes are positive when directed towards the water surface. All terms on the right-hand side of eq. 1 are in W m^{-2}.

Due to poor spatial coverage of both solar and longwave radiation observations across most malaria endemic regions, estimates are therefore required. Hargreaves and Samani (1982) estimated daily solar radiation R_s based on daily maximum and minimum temperature difference given by eq. 2:

$$R_S = R_a K \sqrt{(T_{\max} - T_{\min})} \qquad \text{(eq. 2)}$$

where: R_a is extra-terrestrial radiation (W m^{-2}); T_{max} and T_{min} are daily maximum and minimum 2 metre air (K), respectively; and K empirical coefficient (K$^{-0.5}$).

Hargreaves (1994) suggested K values of 0.16 and 0.19K$^{-0.5}$ for interior and coastal regions, respectively. In this study the location is assumed to be interior.

The extra-terrestrial radiation R_a was computed following Iqbal (1983):

$$R_a = I_{sc} E_o (\sin\delta\sin\phi + \cos\delta\cos\phi\cos\omega_i) \qquad \text{(eq. 3)}$$

where: I_{sc} is the solar constant (1353 W m^{-2}); E_o is the eccentricity correction; δ is the solar declination; ϕ is the latitude; and w_i is the hour angle at the middle of an hour.

The incoming and outgoing longwave radiations are estimated following Losordo and Piedrahita (1991) and Hodges (1998), which are expressed as the second and third terms on the right-hand side of eq. 4, respectively. The first term on the right-hand side of eq. 4 represents net solar radiation.

Figure 2. Schematic representation of the energy balance model. SH, sensible heat flux; LH, latent heat; SF, shade factor; R$_s$, shortwave solar radiation; ε$_w$, water surface emissivity; T$_a$, air temperature; T$_w$, water temperature; d, water depth; G$_o$, soil heat flux.

$$R_{\text{net}} = (1 - \alpha)(1 - \text{SF})R_s + (1 - r)\varepsilon_a\sigma T_a^4 - \varepsilon_w\sigma T_w^4 \quad \text{(eq. 4)}$$

$$\varepsilon_a = 0.398 \times 10^{-5} T_a^{2.148} \qquad \text{(eq. 5)}$$

where: α stands for the shortwave albedo of water; *SF* is the shade factor; R_s represents the shortwave solar radiation; r is the albedo of water surface to longwave radiation; ε_a is the emissivity of the atmosphere (eq. 5) computed following after (Swinbank, 1963); σ (W m^{-2}) is the Stefan-Boltzmann constant; ε_w is the water surface emissivity; T_w and T_a represent the water and 2 metre air (K), respectively.

The shade factor *SF* ranges from 0 (completely shaded) to 1 (fully sun-lit) to account for the influence of tall vegetation on water temperature (Sinokrot and Stefan, 1993; Younus *et al.*, 2000). Although the model allows for vegetation effects to be included through this simple shade factor, in practice it would be difficult to set a reasonable value for such a factor in regional simulations. The *SF* is set to zero in the simulations conducted here for sunlit ponds.

For non-radioactive components, we used a bulk parameterisation for the turbulent fluxes according to Fischer *et al.* (1979):

$$\text{SH} = \rho_a C_p C_{\text{DH}} U_a (T_w - T_a) \qquad \text{(eq. 6)}$$

$$\text{LH} = \rho_a L_v C_{\text{DE}} U_a (q_w - q_a) \qquad \text{(eq. 7)}$$

where: ρ_a (kg m^{-3}) stands for the air density; C_p (J kg^{-1} K^{-1}) is the specific heat capacity of air at constant pressure; U_a (m s^{-1}) is the wind speed at 10 m height; q_w and q_a are the water surface specific humidity and 2 metre air humidity respectively; L (j kg^{-1}) represents the latent heat of vaporisation.

C_{DH} and C_{DE} are bulk aerodynamic coefficients (Pond *et al.*, 1971; Hicks, 1972). In this study, a constant value of 1.3×10^{-3} is assigned to these constants (Paulson *et al.*, 1972).

The soil heat flux G_o (eq. 1), which is relatively small compared with the other fluxes, is parameterised as a fraction of R$_{net}$ following Liebethal and Foken (2007):

$$G_o = f R_{\text{net}} \qquad \text{(eq. 8)}$$

where *f* is a fractional constant.

As there are no observations of G_o in the field experiment, this term represents one of the key sources of error in the energy balance model. In this study, *f* was set to 0.15 after Paaijmans *et al.* (2008b); which is also close to 0.14 used by Liebethal and Foken (2007). The latter found good agreement of the f value with observations.

As diffusive and convective transport is neglected and temperature is considered uniform in each water body, the prognostic temperature is integrated forward in time using a simple explicit solution (Caissie *et al.*, 2005; Larnier *et al.*, 2010). Paaijmans *et al.* (2008a) used a similar equation to predict water temperature of artificially created ponds:

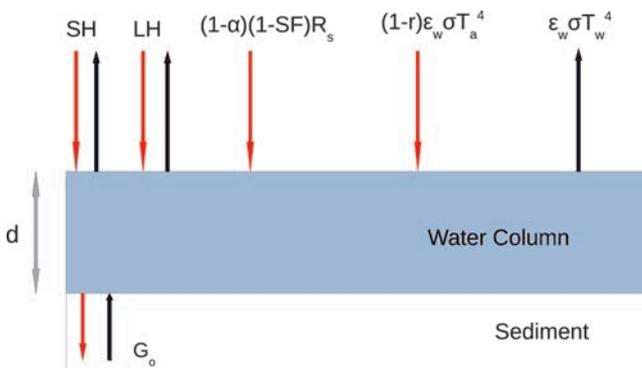$$T_w(t + \Delta t) = T_w(t) + \frac{1}{\rho c_w d}\left(\frac{dQ}{dt}\right)\Delta t \qquad \text{(eq. 9)}$$

where: ρ (kg m^{-3}) is the density of water; C_w (J kg^{-1} K^{-1}) is the specific heat of water at constant pressure; d (m) is the water depth and Δt the time and t the time step used to integrate the equation which is set to one hour.

The water depth (d) was assigned a constant mean value (Torgersen *et al.*, 2001; Dupont and Mestayer, 2006). Furthermore, larvae of the prolific malaria vector *Anopheles gambiae* remain close to the water surface and diving increases its mortality (Tuno *et al.*, 2004). eq. 9 was integrated using the observed pond temperature measurement as the initial temperature.

Vector-borne disease community model of the International Centre for Theoretical Physics, Trieste simulated larval density

Tompkins and Ermert (2013) introduced the Vector-borne disease community model of the International Centre for Theoretical Physics, Trieste (VECTRI). VECTRI is an open source model for malaria that can simulate transmission at a single location, or for a grid of points over a region or even continental scale (Caminade *et al.*, 2014; Pointek *et al.*, 2014; Tompkins and Di Giuseppe, 2015).

VECTRI incorporates larvae growth rate schemes based on degree-day expressed as:

$$R_L = \frac{T_w - T_{\text{L,min}}}{K_L} \qquad \text{(eq. 10)}$$

where: R_L is the growth rate; $T_{L,min}$ is the threshold temperature below, which larval development ceases, and K_L is the degree-days required for adult emergence.

The value of K_L has been estimated from laboratory studies to be 90.9 degree days [Jepson approximation (JA); Jepson *et al.*, 1947] and 200-degree days [Bayoh approximation (BA); Bayoh and Lindsay, 2003]. These two schemes are used to evaluate the difference in VECTRI simulated larvae abundance using simulated water and observed water and air temperatures. For details see Tompkins and Ermert (2013).

Generally, aquatic stage development rate simulations are based on daily average temperature calculated from daily minimum and maximum temperatures $\left(\frac{T_{\text{min}} + T_{\text{max}}}{2}\right)$. However, recent studies showed that diurnal temperature fluctuations significantly influence the duration of larvae development (Carrington *et al.*, 2013; Paaijmans *et al.*, 2013). We further assessed the difference using daily, diurnal (*i.e.*, hourly) and sub-hourly timesteps of water and air temperatures to predict larvae development. For sub-daily timescales, the developmental rate was estimated following Gu and Novak (2006):

$$R_L = \frac{\sum_{i=1}^{N}\left(T_{w,i} - T_{L,min}\right)}{N x K_L} \qquad \text{(eq. 11)}$$

where N is 24 for hourly observations and 144 for 10-min measurements.

Model evaluation

The performance of the model was evaluated using the coefficient of determination (R^2), the Nash-Sutcliffe efficiency (*NSE*) (Nash and Sutcliffe, 1970) and mean bias error (*MBE*) defined by eq. 12:

$$NSE = 1 - \frac{\sum_{i=1}^{N}(O_i - S_i)^2}{\sum_{i=1}^{N}(O_i - \bar{O})^2}$$

$$R^2 = \left(\frac{\sum_{i=1}^{N}(O_i - \bar{O})(S_i - \bar{S})}{\sqrt{\sum_{i=1}^{N}(O_i - \bar{O})^2 \sum_{i=1}^{N}(S_i - \bar{S})^2}}\right)^2 \qquad \text{(eq. 12)}$$

$$MBE = \frac{1}{N}\sum_{i=1}^{N} O_i - S_i$$

where: S_i refers to the i_{th}-simulated value; O_i is the i_{th} observation; $\bar{O}$ and $\bar{S}$ are the mean of observed and simulated data values, respectively; and N is the total number of observations.

The NSE ranges between $-\infty$ and 1 (perfect model), and indicates how well a scatter plot of model versus observation fits a 1:1 line. The NSE values ≤ 0.0 implies unacceptable model performance.

Results

Observed water temperature variability

Figure 3A-C shows water temperature variability of the three monitored mosquito developmental habitats. The mean 10-min maximum and minimum water temperatures were 34.2°C (range: 26.2 to 39.3°C) and 24.0°C (range: 21.6 to 25.5°C), respectively. On a daily timescale, the mean, maximum and minimum water temperatures were 27.2, 29.2 and 24.0°C, respectively.

During the same period, the average mean, maximum and minimum air temperatures measured from the AWS were 29.7°C (range: 23.5 to 33.0°C) and 21.9°C (range: 19.5 to 23.5°C) respectively. The daily average mean, maximum and minimum air temperatures were 24.9, 27.5 and 22.4°C, respectively. The differences between the diurnal water and air temperatures are shown in Figure 3D-F for the three observed sites. Generally, as expected water temperatures were higher relative to air temperatures. The highest differences between water and air temperatures occurred generally in the afternoon hours. By contrast, few observations existed where air temperatures exceeded water temperatures. This is the case in the morning hours between about 8 and 12 GMT at the end of the study period. The average mean, maximum and minimum differences between water and air temperatures were 2.4, 11.8 and 0.0°C, respectively. However, for the period where air temperatures were higher than water temperatures, the average mean, maximum and minimum temperature differences were 0.5, 2.0 and 0.0°C, respectively.

Furthermore, Figure 3A-C reveals that rainfall variability controls temporary surface water stability. The gaps in the time series are dry periods. The average water depths are about 14, 10 and 5 cm for sites 1, 2 and 3, respectively.

Figure 4 shows time series of diurnal water temperature range (DTR) (daily maximum minus daily minimum) and the daily average water and air temperature difference. Contrary to the hourly difference in water and air temperatures (Figure 3D-F), the daily average water temperatures were consistently higher than the air temperatures. The daily average, maximum and minimum differences are 2.3, 4.3 and

0.9°C, respectively. In addition, the ponds exhibit high DTR, implying that mosquito larvae are exposed to highly variable temperatures. The mean, maximum and minimum DTR are 10.1, 14.9 and 4.2°C, respectively. Paaijmans *et al.* (2008a) observed similar DTR values of 14.4 and 7.1°C for smaller and larger sized artificially created ponds in Kenya.

The maximum number of hours per day with water temperature higher than or equal to 35°C was 5 h, with average of about 1.7 h (Figure 5). Interestingly, larvae were observed (visual inspection) in

the habitats throughout the observational period despite maximum temperature of excess of 35°C encountered.

Model output

Figure 6A-C show the diurnal observed and simulated temperature differences (observed minus simulated), and the scatter plots of the diurnal simulated compared with observed temperatures are shown in Figure 6G-I. The resulting daily average time series of simulated,
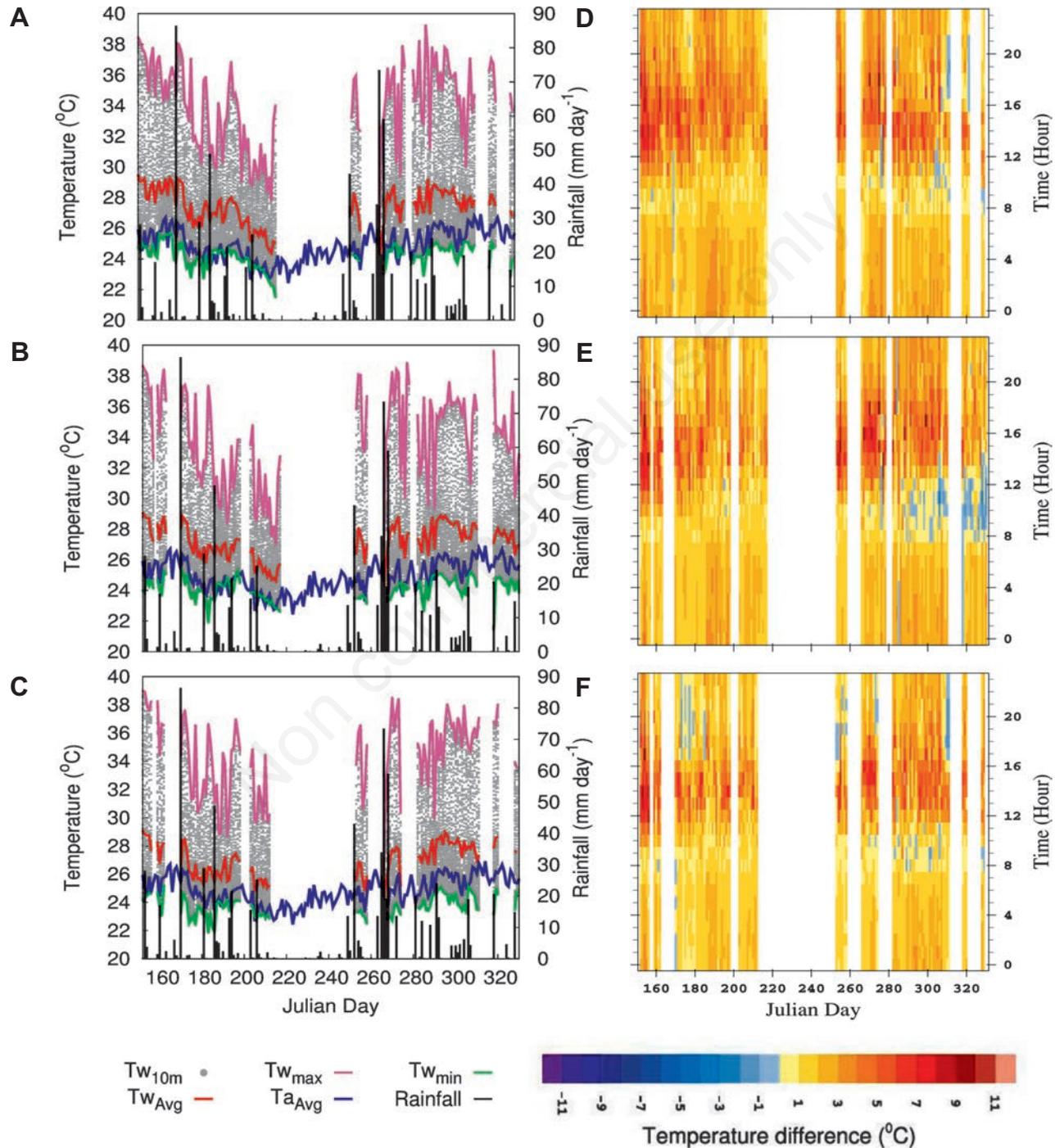

Figure 3. A-C) Observed 10-min (Tw$_{10m}$), maximum (Tw$_{max}$), minimum (Tw$_{min}$), daily average (Tw$_{Avg}$) water temperatures and daily average air (Ta$_{Avg}$) temperature. D-F) Diurnal temperature difference (water minus air). The A,D), B,E) and C, F) panels represent sites 1, 2 and 3, respectively.

observed and air temperatures are shown in Figure 6D-F. The diurnal pattern of bias (Figure 6A-C) demonstrates a relatively good agreement between model and observations. The average *NSE*, *R²* and *MBE* are 0.768, 0.888 and –0.191°C (Table 1), respectively. However, in most cases, the model overestimates the observed water temperature in the late evening and early morning before sunrise (Figure 6A-C) but slightly underestimates it outside this time range. Due to this under/overestimation on hourly scale, the daily average model and observed water temperature show good agreement (Figure 6D-F). The average *NSE*, *R²* and *MBE* are 0.587, 0.814 and –0.187°C (Table 1), respectively.

Larvae development time

The JA and BA schemes predicted mosquito larvae development time using observed water (site 1), simulated water and observed air temperatures between the period 152 and 217 DOY are compared. Site 1 was selected because it contained water throughout this period.

To assess the importance of sub-daily temperature variability in larvae development, 10-min, hourly and daily average observed water and air temperatures driven aquatic development duration are compared (Figure 7). There was a remarkably close match between predicted larvae development time at 10-min and hourly timescales for both water and air temperatures. However, daily average temperatures (both water and air) consistently predicted a faster aquatic stage development relative to both the 10-min and hourly observations. The average difference of simulated larvae lifespan between daily and 10-min timescales is about 8.8% (air temperature) and 13.6% (water temperature) for both schemes. These differences resulted in *MBE* of about (JA: 1 day; BA: 2 days) for both water and air temperatures. Similar developmental times were observed at daily and hourly timescales.

Due to similar developmental times predicted from both 10-min and hourly timescales, the model is run with an hourly time step. Generally, there were was an agreement between larvae developmental time predictions from observed and simulated water temperatures from both schemes (Figure 8). The *NSE* (JA: 0.766; BA: 0.766), *R²* (JA; 0.905; BA: 0.905) and *MBE* (JA: –0.142 days; BA: –0.313 days) values were computed for observed and simulated water driven larvae developmental time simulations. As expected, the schemes driven by air temperature constantly predicted longer development time relative to both the observed and simulated water temperatures (Figure 8). This resulted in negative *NSE* (JA: –5.094; BA: –5.094) and large *MBE* (JA: –2.445 days; BA: –5.379 days) values between observed water and air temperatures simulated larvae duration time. On the other hand, a high *R²* value 0.900 was observed between predicted larvae development time using air and observed water temperatures indicating that these two variables reveal a similar trend.

Vector-borne disease community model of the International Centre for Theoretical Physics, Trieste simulated larvae density

The 7-day moving average time series of the VECTRI simulated larvae density from the two schemes and water fraction are shown in
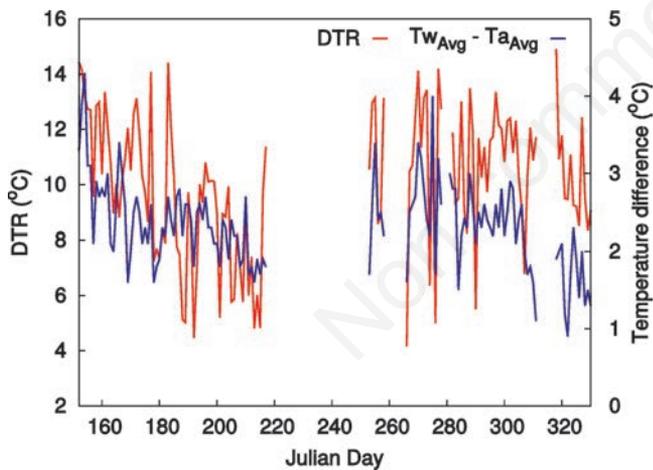

Figure 4. Comparison of daily water temperature range (DTR) and daily average (Avg) temperature difference (water minus air).
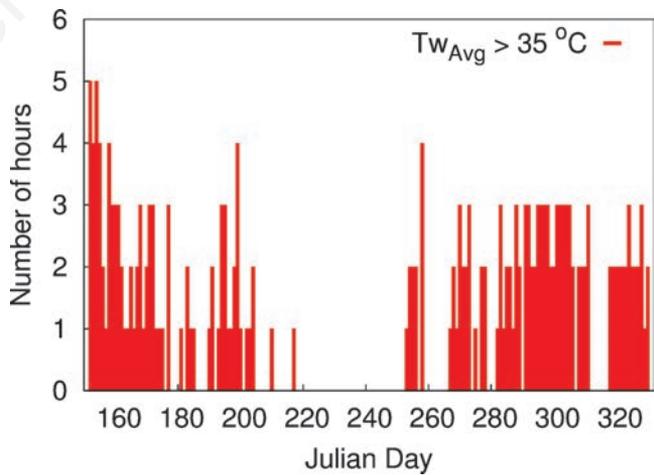

Figure 5. Daily number of hours with water temperature (T) ≥35°C. Avg, average.

Table 1. Summary of the computed statistics for model evaluation.

	Diurnal temperature			Daily temperature			LD (T$_{obs}$/T$_{sim}$)		LD (T$_{obs}$/T$_{air}$)	
	Site 1	Site 2	Site 3	Site 1	Site 2	Site 3	JA	BA	JA	BA
R²	0.902	0.889	0.872	0.852	0.790	0.801	0.905	0.905	0.900	0.900
NSE	0.802	0.771	0.733	0.706	0.545	0.508	0.766	0.766	–5.094	–5.095
MBE	–0.003	–0.102	–0.468	–0.026	–0.119	–0.417	–0.142	–0.313	–2.445	–5.379

LD (T$_{obs}$/T$_{sim}$), larvae development time between observed and simulated water temperatures; LD (T$_{obs}$/T$_{air}$), larvae development time between observed water and air temperatures; JA, Jepson approximation; BA, Bayoh approximation; R², coefficient of determination; NSE, Nash-Sutcliffe efficiency; MBE, mean bias error.

Figure 9. The mean modelled water temperature is 27.2°C, about 9% more than mean observed air temperature of 24.9°C. This difference in temperature also impacts VECTRI simulated larvae density. As expected mean larvae density from modelled water temperature driven simulations were higher relative to the air temperature driven simulations. In addition, we observed significant differences in the simulated larvae density between water and air temperatures for the two schemes. For example, while JA scheme (Figure 9) predicted a mean larvae density difference of about 18% between modelled water and observed air temperatures as input for VECTRI, the BA scheme predicted a difference of about 71% (Figure 9).

VECTRI simulates also the pond water fraction, which limits larval density. The ponds dried out between the Julian days 218 and 252. VEC-TRI simulates the minimum in the water fraction somewhat later and for a shorter period (*i.e.*, between 230 and 250 DOY). Interestingly, this coincides with the period with a close match between the larval development schemes simulated larval densities. In VECTRI a close link exists between water fraction and larvae density; as water fraction reduces, the larvae density also reduces as larvae are instantaneously killed once the pond dries out (Tompkins and Ermert, 2013).

Discussion

This study has revealed that water temperatures of temporary bodies of surface water are highly variable. Colonising mosquito larvae would be exposed to temperatures ranging from about 21.6 up to 39.3°C, with a daily average of 27.2°C. This observed mean temperature is within the optimal temperature range for aquatic stage development based on
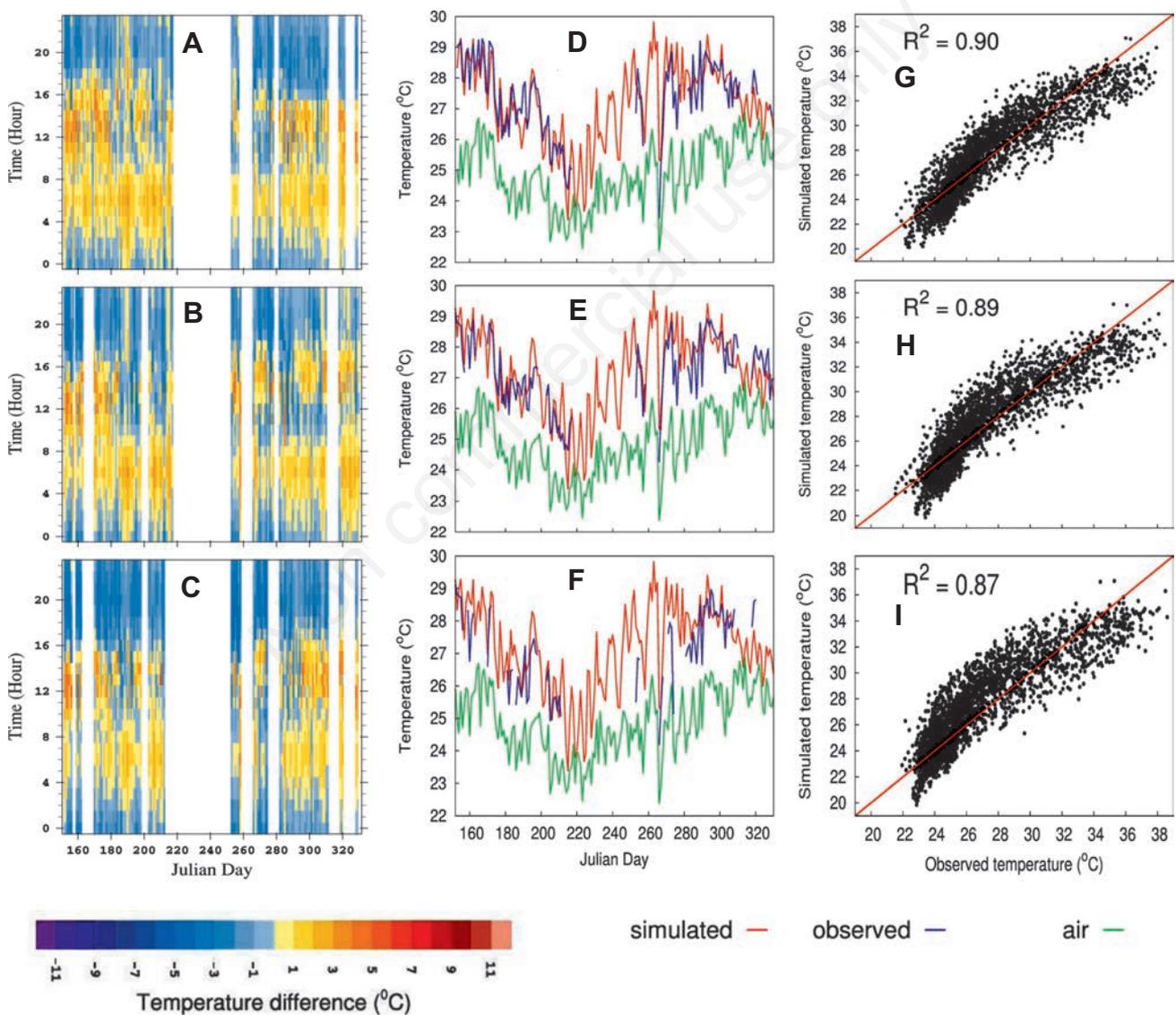

Figure 6. A-C) Comparison of the diurnal observed and simulated temperature differences (observed minus simulated) and (D-F) daily average time series of air, observed and model water temperatures. Also shown is correlation between observed and simulated diurnal water temperatures (G-I). The A,D,G), B,E,H) and C,F,I) panels represent sites 1, 2 and 3, respectively.

laboratory studies (Lyimo *et al.*, 1992; Bayoh, 2001; Bayoh and Lindsay, 2003). Similar ranges of pond temperatures have been reported elsewhere. For instance, in western Kenya, Koenraadt *et al.* (2004) observed mean, maximum and minimum temperatures of about 28.0, 37.4 and 14.6°C respectively from field measurements. In Gambia, Bayoh (2001) observed temperature range between 20.7 and 36.9°C with mean of 27.1°C from artificially created pond measurements. Similarly, three artificially created ponds of different dimension and depth in western Kenya, Paaijmans *et al.* (2008a) observed mean water temperature between 27.4 and 28.1°C. Furthermore, these observed temperatures are likely to support larvae development as a similar range found elsewhere supported full larvae development (Gouagna *et al.*, 2012; Mwangangi *et al.*, 2007).

The observed minimum water temperature from these three potential mosquito developmental habitats were higher than the minimum threshold temperature of 16°C that supports larvae development under constant temperature in laboratory experiments (Bayoh and Lindsay, 2003). On the other hand, despite the water temperature exceeding the upper temperature limit of 35°C reported from laboratory studies (Bayoh and Lindsay, 2003), the water temperature threshold of 41°C, lethal to larvae even over a short period (Haddow, 1943), was never encountered. In addition, larvae are likely to survive the maximum number of 5 h per day with water above or equal to 35°C. For instance, Kirby and Lindsay (2009) observed larvae to adult development at 35°C when larvae were reared at fixed temperatures.

The results from the evaluation of the energy balance scheme reveal that despite the simplified assumptions made to derive estimates of energy fluxes, the model reproduces the observed diurnal water temperature values quite well. However, it mostly overestimates the observed water temperature during early morning before sunrise and late evening during the period of lower observed water temperatures (Figure 6G-I). This could be due to the presences of nocturnal clouds observed during monsoon period over West Africa, including Kumasi

(Schrage *et al.*, 2007; Knippertz *et al.*, 2011). These low clouds increase the surface temperature at night. Since surface temperature was used instead of top of the atmosphere temperature to estimate the downward longwave radiation, this could lead to a slight overestimation of the downward longwave radiation at this time of the day.

Furthermore, the lower performance of the model for site 3 could be due to its shallow water depth. This results in a high water temperature variability. A diurnal water temperature model (Paaijmans *et al.*, 2008a) performed less well in predicting water temperature of a shallow pond with a depth of 4 cm relative to ponds with depths of 16 and 32 cm. Despite this, our model underestimates the observed water temperatures slightly, as given by the *MBE* values (Table 1). In addition, based on *NSE* and R^2 evaluation metrics, the model performed well in representing the observed water temperatures.

In addition, aquatic stage lifespan simulations at various timescales reveal the importance of sub-daily variability. This is in agreement with other studies (Carrington *et al.*, 2013; Paaijmans *et al.*, 2013). Our results, however, indicate that temperature fluctuations below hourly timescale have little to no effect on larvae development rate (Figure 7). As a result, an hourly time step model could accurately predict aquatic stage development times. There was a good agreement between observed and simulated water temperatures predicted larvae developmental times (Figure 8), with mean difference of about 1.72%. Furthermore, the mean estimated larvae development time (8.2 days: observed water; 8.4 days: simulated water) from the JA scheme is approximately equal to mean 8.4 days observed by Gimnig *et al.* (2002) when 20 larvae were reared in artificial habitats without nutrients in western Kenya. In addition to this, the range of JA scheme estimated development times (6.7-10.8 days: observed water; 6.8-12.3 days: simulated water) are within their observed range of days when different numbers of larvae were reared. This agreement maybe due to the almost similar range of temperatures they observed (24.6°C: average minimum; 36.0°C: average maximum). In the laboratory, when larvae
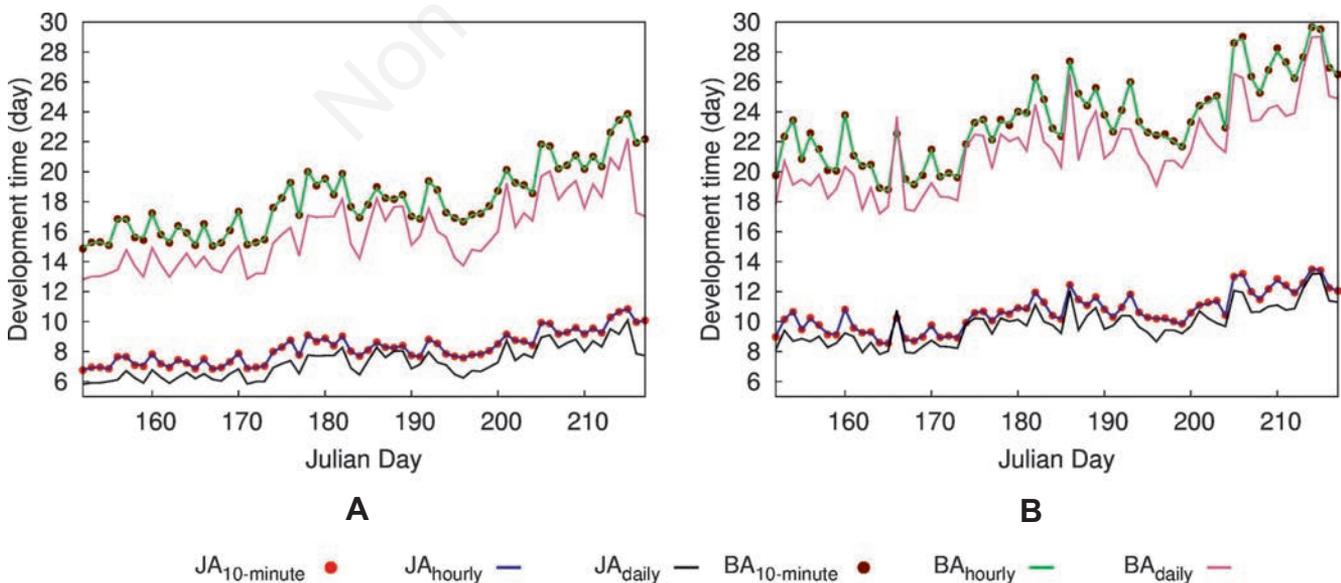
Figure 7. Comparison of Jepson approximation (JA) and Bayoh approximation (BA) schemes estimated mosquito larvae development time using observed 10-min ($_{10\text{-min}}$), hourly ($_{hourly}$) and daily ($_{daily}$) average water (A) and air (B) temperatures.

were reared at constant temperatures of 24, 27 and 30°C, Lyimo *et al.* (1992) observed age to pupation ranges between 6 to 17 days, with an average of 9.79 days. Although longer development times have been reported elsewhere (Minakawa *et al.*, 2006; Munga *et al.*, 2006), their observed temperature ranges were lower relative to the water temperatures we observed. This clearly demonstrates the potential of this simplified scheme to reliably predict aquatic stage development times of mosquito.

As expected, air temperature predicted longer larvae duration time with mean difference of about 2.3 days (equivalent to 29.67%) relative to the observed water temperature. In western Kenya, Paaijmans *et al.* (2010) observed similar high differences in larvae development times of 25-28% using air and water temperatures. Their observed mean air temperature of 23.4°C is close to the 24.9°C we observed. However, in the same study, they observed higher differences, ranging between 39-45% for two highland towns, with a lower mean air temperature of about 19°C. These results reveal that models using air temperature to simulate larvae development overestimate larvae development time. In addition, though the high R^2 indicates similar trends between observed water and air temperatures, the negative *NSE* values indicate poor performance using air temperature to predict larvae development.

Comparing the larvae duration time predicted from these two schemes reveals the importance of the K_L parameter. The JA scheme driven by air temperature predicted faster larvae development relative to the BA scheme driven by both observed and simulated water temperatures (Figure 8). This suggests that water temperature and K_L are two key important variables for the accurate simulation of the larvae development time.

The VECTRI simulation results highlight the nonlinearity of the relationship between temperature and larvae development rate. The percentage difference between modelled water and observed air temperatures did not produce the same percentage change in the VECTRI simulated larvae density. Pascual *et al.* (2006) and Bayoh and Lindsay (2003) also found a nonlinear relation between change in climate variables and mosquito population dynamics. In addition, the large disparity between larval densities simulated by the schemes clearly shows the

importance of the K_L term. This highlights the fact that the challenge of modelling the aquatic stage of the life cycle of mosquitoes arises not only from difficulties in accurately representing water temperature per se but also the K_L term.

Conclusions

We developed a simple energy balance model to predict hourly and daily water temperatures as well as larvae development times and evaluated the model *via in situ* pond observations. We found that the simulated water temperatures are similar to observations of three ponds in Kumasi, Ghana. Just only observed minimum and maximum air temperatures from common weather stations are required to model realistic water temperatures. Our study reveals also that disease models should not apply air temperatures as water temperatures.

Incorporating the developed water temperature scheme in vector-borne disease models will likely contribute significantly to the improvement of disease simulations such as for malaria forecasts. For example, the implementation of our simple energy balance model into weather-driven dynamical malaria models will likely improve the simulation of the malaria transmission cycle. Earlier malaria transmission cycles would be the result from the use of the water temperature scheme. In addition, our findings imply that improved degree-day development time larval schemes are required for realistic larval growth simulations.

Despite this, difficulty still remains in applying the scheme on a regional scale. The challenge of modelling the mean water temperature of the aggregate ponds within each grid-cell (*e.g.*, 10×10 km), taking into account the impact of vegetation coverage, as well as ponds of different sizes and depths on water temperature is the subject of current work. Furthermore, availability of a longer dataset would be useful to assess the model performance. However, our study is an important contribution towards the improvement of weather-driven dynamical vector-borne disease models that could be applied in the near future as decision tools for disease programmes.
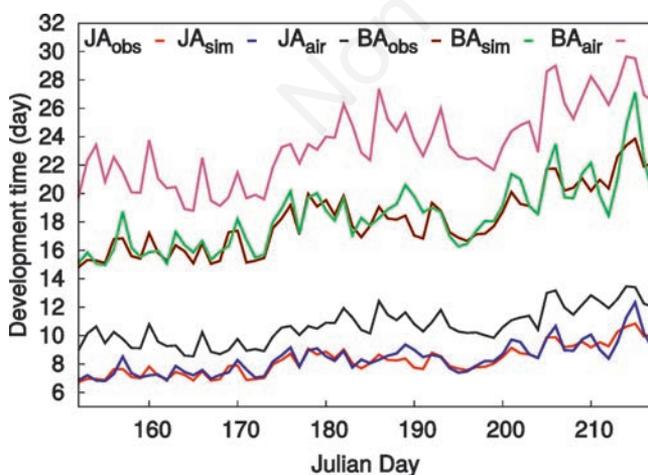

Figure 8. Comparison of Jepson approximation (JA) and Bayoh approximation (BA) schemes estimated mosquito larvae development time using observed water (obs), simulated water (sim) and air temperatures (air).
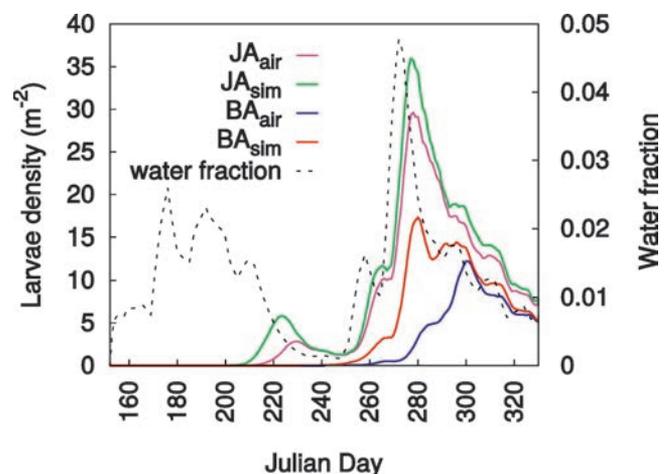

Figure 9. Comparison of 7-day moving average time series of Vector-borne disease community model of the Abdus Salam International Centre for Theoretical Physics, Trieste simulated larvae density driven by air and simulated water temperatures using Jepson approximation (JA) and Bayoh approximation (BA) schemes.

References

Bayoh M, Lindsay S, 2003. Effect of temperature on the development of the aquatic stages of *Anopheles gambiae sensu stricto* (Diptera: Culicidae). Bull Entomol Res 93:375-82.

Bayoh M, Lindsay S, 2004. Temperature-related duration of aquatic stages of the Afrotropical malaria vector mosquito *Anopheles gambiae* in the laboratory. Med Vet Entomol 18:174-9.

Bayoh MN, 2001. Studies on the development and survival of *Anopheles gambiae sensu stricto* at various temperatures and relative humidities. PhD Thesis; University of Durham, UK.

Caissie D, Satish MG, El-Jabi N, 2005. Predicting river water temperatures using the equilibrium temperature concept with application on Miramichi River catchments (New Brunswick, Canada). Hydrol Processes 19:2137-59.

Caminade C, Kovats S, Rocklov J, Tompkins AM, Morse AP, Colón-González FJ, Stenlund H, Martens P, Lloyd SJ, 2014. Impact of climate change on global malaria distribution. P Natl Acad Sci USA 111:3286-91.

Carrington LB, Armijos MV, Lambrechts L, Barker CM, Scott TW, 2013. Effects of fluctuating daily temperatures at critical thermal extremes on *Aedes aegypti* life-history traits. PLoS One 8:e58824.

Craig M, Snow R, Le Sueur D, 1999. A climate-based distribution model of malaria transmission in sub-Saharan Africa. Parasitol Today 15:105-11.

De Souza D, Kelly-Hope L, Lawson B, Wilson M, Boakye D, 2010. Environmental factors associated with the distribution of Anopheles gambiae ss in Ghana; an important vector of lymphatic filariasis and malaria. PLoS One 5:e9927.

Depinay JMO, Mbogo CM, Killeen G, Knols B, Beier J, Carlson J, Dushoff J, Billingsley P, Mwambi H, Githure J, Toure AM, McKenzie FE, 2004. A simulation model of African Anopheles ecology and population dynamics for the analysis of malaria transmission. Malaria J 3:29.

Detinova T, 1962. Age-grouping methods in Diptera of medical importance: with special reference to some vectors of malaria. Monograph series 47. World Health Organization (WHO), Geneva, Switzerland, pp 13.

Dupont S, Mestayer PG, 2006. Parameterization of the urban energy budget with the sub-mesoscale soil model. J Appl Meteor Climatol 45:1744-65.

Ermert V, Fink AH, Jones AE, Morse AP, 2011a. Development of a new version of the Liverpool malaria model. I. Refining the parameter settings and mathematical formulation of basic processes based on a literature review. Malaria J 10:35.

Ermert V, Fink AH, Jones AE, Morse AP, 2011b. Development of a new version of the Liverpool malaria model. II. Calibration and validation for West Africa. Malaria J 10:62.

Fischer HB, List EJ, Koh RCY, Imberger J, Brooks NJ, 1979. Mixing in inland and coastal waters. Academic Press, New York, NY, USA.

Garrett-Jones C, Grab B, 1964. The assessment of insecticidal impact on the malaria mosquito's vectorial capacity, from data on the proportion of parous females. Bull World Health Org 31:71.

Gimnig JE, Ombok M, Kamau L, Hawley WA, 2001. Characteristics of larval anopheline (Diptera: Culicidae) habitats in Western Kenya. J Med Entomol 38:282-8.

Gimnig JE, Ombok M, Otieno S, Kaufman MG, Vulule JM, Walker ED, 2002. Density-dependent development of *Anopheles gambiae* (Diptera: Culicidae) larvae in artificial habitats. J Med Entomol 39:162-72.

Gosnell R, Fairall C, Webster P, 1995. The sensible heat of rainfall in the tropical ocean. J Geophys Res 100:18437-42.

Gouagna LC, Rakotondranary M, Boyer S, Lempérière G, Dehecq JS, Fontenille D, 2012. Abiotic and biotic factors associated with the presence of *Anopheles arabiensis* immatures and their abundance in naturally occurring and man-made aquatic habitats. Parasite Vector 5:96.

Gu W, Novak RJ, 2006. Statistical estimation of degree days of mosquito development under fluctuating temperatures in the field. J Vector Ecol 31:107-12.

Haddow A, 1943. Measurements of temperature and light in artificial pools with reference to the larval habitat of *Anopheles* (Myzomyia) *gambiae*, Giles, and *A.* (M.) *funestus*, Giles. Bull Entomol Res 34:89-93.

Hargreaves G, 1994. Simplified coefficients for estimating monthly solar radiation in North America and Europe. Departmental paper; Department of Biological and Irrigation Engineering, Utah State University, Logan, UT, USA.

Hargreaves GH, Samani ZA, 1982. Estimating potential evapotranspiration. J Irrig Drain Div Am Soc Civ Eng 108:225-30.

Hicks B, 1972. Some evaluations of drag and bulk transfer coefficients over water bodies of different sizes. Bound-Lay Meteorol 3:201-13.

Hodges B, 1998. Heat budget and thermodynamics at a free surface: some theory and numerical implementation. Centre for Water Research, University of Western Australia, Crawley, WA, Australia.

Hoshen MB, Morse AP, 2004. A weather-driven model of malaria transmission. Malaria J 3:32.

Iqbal M, 1983. An introduction to solar radiation. Academic Press, Toronto, Canada, pp 41-65.

Jepson W, Moutia A, Courtois C, 1947. The malaria problem in Mauritius: the bionomics of Mauritian anophelines. Bull Entomol Res 38:177-208.

Kirby MJ, Lindsay SW, 2004. Responses of adult mosquitoes of two sibling species, *Anopheles arabiensis* and *A. gambiae* ss (Diptera: Culicidae), to high temperatures. Bull Entomol Res 94:441-8.

Kirby MJ, Lindsay SW, 2009. Effect of temperature and inter-specific competition on the development and survival of *Anopheles gambiae sensu stricto* and *An. arabiensis* larvae. Acta Trop 109:118-23.

Knippertz P, Fink AH, Schuster R, Trentmann J, Schrage JM, Yorke C, 2011. Ultra-low clouds over the southern West African monsoon region. Geophys Res Lett 38:L21808.

Koenraadt C, Githeko A, Takken W, 2004. The effects of rainfall and evapotranspiration on the temporal dynamics of *Anopheles gambiae* ss and *Anopheles arabiensis* in a Kenyan village. Acta Tropica 90:141-53.

Larnier K, Roux H, Dartus D, Croze O, 2010. Water temperature modeling in the Garonne River (France). Knowl Manage Aquat Ecosyst 398:4.

Liebethal C, Foken T, 2007. Evaluation of six parameterization approaches for the ground heat flux. Theor Appl Climatol 88:43-56.

Losordo TM, Piedrahita RH, 1991. Modelling temperature variation and thermal stratification in shallow aquaculture ponds. Ecol Model 54:189-226.

Lunde TM, Bayoh MN, Lindtjørn B, 2013a. How malaria models relate temperature to malaria transmission. Parasite Vector 6:20.

Lunde TM, Korecha D, Loha E, Sorteberg A, Lindtjørn B, 2013b. A dynamic model of some malaria-transmitting anopheline mosquitoes of the Afrotropical region. I. Model description and sensitivity analysis. Malaria J 12:28.

Lyimo E, Takken W, Koella J, 1992. Effect of rearing temperature and larval density on larval survival, age at pupation and adult size of

Anopheles gambiae. Entomol Exp Appl 63:265-71.

Minakawa N, Mutero CM, Githure JI, Beier JC, Yan G, 1999. Spatial distribution and habitat characterization of anopheline mosquito larvae in Western Kenya. Am J Trop Med Hyg 61:1010-6.

Minakawa N, Omukunda E, Zhou G, Githeko A, Yan G, 2006. Malaria vector productivity in relation to the highland environment in Kenya. Am J Trop Med Hyg 75:448-53.

Munga S, Minakawa N, Zhou G, Mushinzimana E, Barrack OOJ, Githeko AK, Yan G, 2006. Association between land cover and habitat productivity of malaria vectors in western Kenyan highlands. Am J Trop Med Hyg 74:69.

Mwangangi JM, Muturi EJ, Shililu JI, Muriu S, Jacob B, Kabiru EW, Mbogo, CM, Githure, JI, Novak, RJ, 2007. Environmental covariates of *Anopheles arabiensis* in a rice agroecosystem in Mwea, Central Kenya. J Am Mosq Control Assoc 23:371-7.

Nash J, Sutcliffe J, 1970. River flow forecasting through conceptual models part I-A discussion of principles. J Hydrol 10:282-90.

Paaijmans K, Jacobs A, Takken W, Heusinkveld B, Githeko A, Dicke M, Holtslag A, 2008a. Observations and model estimates of diurnal water temperature dynamics in mosquito breeding sites in western Kenya. Hydrol Proces 22:4789-801.

Paaijmans KP, Heinig RL, Seliga RA, Blanford JI, Blanford S, Murdock CC, Thomas MB, 2013. Temperature variation makes ectotherms more sensitive to climate change. Glob Change Biol 19:2373-80.

Paaijmans KP, Heusinkveld BG, Jacobs AF, 2008b. A simplified model to predict diurnal water temperature dynamics in a shallow tropical water pool. Int J Biometeorol 52:797-803.

Paaijmans KP, Imbahale SS, Thomas MB, Takken W, 2010. Relevant microclimate for determining the development rate of malaria mosquitoes and possible implications of climate change. Malaria J 9:196.

Paaijmans KP, Thomas MB, 2013. Relevant temperatures in mosquito and malaria biology. In: W. Takken and C.J.M. Koenraadt (Eds.), Ecology of parasite-vector interactions. Springer, Wageningen, The Netherlands, pp 103-121.

Pascual M, Ahumada J, Chaves L, Rodo X, Bouma M, 2006. Malaria resurgence in the East African highlands: temperature trends revisited. P Natl Acad Sci USA 103:5829-34.

Paulson CA, Leavitt E, Fleagle R, 1972. Air-sea transfer of momentum, heat and water determined from profile measurements during BOMEX. J Phys Oceanogr 2:487-97.

Pointek F, Müllera C, Pugh T, Clark D, Deryng D, Elliott J, Colón-González FJ, Flörke M, Folberth C, Franssen W, Frielera K, Friend AD, Gosling SN, Hemming D, Khabarov N, Kim H, Lomas MR, Masaki Y, Mengel M, Morse A, Neumann K, Nishina K, Ostberg S, Pavlick R, Ruane AC, Schewe J, Schmid E, Stacke T, Tang Q, Tessler ZD, Tompkins AM, Warszawski L, Wisser D, Schellnhuber HJ, 2014. Multisectoral climate impact hotspots in a warming world. P Natl Acad Sci USA 111:3233-8.

Pond S, Phelps G, Paquin J, McBean G, Stewart R, 1971. Measurements of the turbulent fluxes of momentum, moisture and sensible heat over the ocean. J Atmos Sci 28:901-17.

Schrage JM, Augustyn S, Fink A, 2007. Nocturnal stratiform cloudiness during the West African monsoon. Meteorol Atmos Phys 95:73-86.

Sinokrot BA, Stefan HG, 1993. Stream temperature dynamics: measurements and modeling. Water Resour Res 29:2299-312.

Swinbank WC, 1963. Long-wave radiation from clear skies. Q J R Meteorol Soc 89:339-48.

Tompkins AM, Di Giuseppe F, 2015. Potential predictability of malaria in Africa using ECMWF monthly and seasonal climate forecasts. J Appl Meteor Climatol 54:521-40.

Tompkins AM, Ermert V, 2013. A regional-scale, high resolution dynamical malaria model that accounts for population density, climate and surface hydrology. Malaria J 12:65.

Torgersen CE, Faux RN, McIntosh BA, Poage NJ, Norton DJ, 2001. Airborne thermal remote sensing for water temperature assessment in rivers and streams. Remote Sens Environ 76:386-98.

Tuno N, Miki K, Minakawa N, Githeko A, Yan G, Takagi M, 2004. Diving ability of *Anopheles gambiae* (Diptera: Culicidae) larvae. J Med Entomol 41:810-12.

Younus M, Hondzo M, Engel B, 2000. Stream temperature dynamics in upland agricultural watersheds. J Environ Eng 126:518-26.